Available online at www.sciencedirect.com
ScienceDirect
Journal of Nuclear Materials 367–370 (2007) 417–422
journal of nuclear materials
www.elsevier.com/locate/jnucmat

The transport and fate of helium in martensitic steels at fusion relevant He/dpa ratios and dpa rates

R.J. Kurtz [a,*], G.R. Odette [b], T. Yamamoto [b], D.S. Gelles [a], P. Miao [b], B.M. Oliver [a]

[a] *Pacific Northwest National Laboratory, P.O. Box 999, Mail Stop P8-15, Richland, WA 99354, USA*
[b] *University of California, Santa Barbara, CA 93106-5070, USA*

Abstract

Understanding, modeling and managing the effects of He and displacement damage on microstructural evolution and property changes are primary objectives of fusion materials research. We recently implemented an approach for producing controlled He-to-dpa ratios under neutron irradiation using a novel α-implantation technique. Thin 1–4 μm NiAl coatings were deposited on Eurofer-97 TEM discs to produce a uniform He deposition zone of 6–8 μm. The test matrix is aimed at characterizing the transport, fate and consequences of He and He-to-dpa ratio variation on alloys with a wide range of starting microstructure. We explore the effect He-to-dpa ratio and temperature on the microstructure of conventionally processed Eurofer-97. Bubbles were found at all irradiation temperatures, with estimated maximum diameters of ~12, 6.9 and 1.4 nm at 500 °C (~9 dpa and 372 appm He), 400 °C (~3.9 dpa and 82 appm He) and 300 °C (~3.9 dpa and 89 appm He), respectively.

1. Introduction

High concentrations of He will be produced in fusion neutron environments by transmutation reactions. The high-temperature mechanical properties of structural materials will be significantly impacted if He is allowed to aggregate at grain boundaries. It is difficult to explore the effects of He under prototypic conditions due to a lack of appropriate irradiation facilities. To design, develop and validate He resistant microstructures, appropriate experimental methods are needed to introduce He into a material at fusion relevant He-to-dpa ratios. Some methods for producing He in ferritic alloys such as B and Ni doping cause undesirable effects since the composition of the alloy is changed, potentially leading to the formation of atypical phases during irradiation. Isotopic tailoring of ferritic alloys with ^{54}Fe is an attractive approach for simulating He effects in Fe-based materials, but ^{54}Fe is costly and ultimately does not produce the correct He-to-dpa ratio. An alternative method that avoids the limitations of the above approaches is application of a surface layer that under neutron irradiation injects He into the adjacent material [1–3]. Under mixed spectrum neutron irradiation

* Corresponding author. Tel.: +1 509 373 7515; fax: +1 509 376 0418.
E-mail address: rj.kurtz@pnl.gov (R.J. Kurtz).

0022-3115/$ - see front matter © 2007 Elsevier B.V. All rights reserved.
doi:10.1016/j.jnucmat.2007.03.121

conditions the deposition of a Ni bearing coating on any substrate results in α-implantation due to $^{58}Ni(n_{th},\gamma) \rightarrow {}^{59}Ni(n_{th},\alpha)$ reactions. With this approach it is possible to explore the effects of He on microstructural development by implanting He at almost any desired He-to-dpa ratio to a uniform depth of a few microns. Further details of the procedure are given in a companion paper [3].

The objectives of the present study are to (1) characterize the transport, fate and consequences of He and the effects of He-to-dpa ratio variations for alloys with a wide range of starting microstructure; (2) explore the effect of He-to-dpa ratio and irradiation temperature on the microstructure of Eurofer-97 and compare the results to other reduced activation ferritic/martensitic steels, nanostructured ferritic alloys, and various model alloys; and (3) utilize nano-indentation techniques to assess the effects of He on radiation induced strength changes. In the present work we report initial microstructural characterization of He-injected Eurofer-97 TEM discs irradiated at 300, 400 and 500 °C to doses of either 3.9 or 9 dpa in the peripheral target position in the High Flux Isotope Reactor (HFIR). The He-to-dpa ratios investigated were either 21 appm He/dpa at 300 and 400 °C, or 41 appm He/dpa at 500 °C.

2. Experimental

The HFIR JP26 irradiation experiment contained a series of transmission electron microscopy (TEM) disks intended to study helium effects in ferritic/martensitic steels [4,5]. Table 1 lists specimens chosen for examination. The Eurofer-97 disks were prepared with thin NiAl coatings so that irradiation would produce He by transmutation of the Ni and deposit that He uniformly in a thin layer ~6 to 8 μm thick adjacent to the coating. Yamamoto et al. [3] give details of the specimen design and preparation. Following irradiation, samples were prepared for TEM using a cross-section technique to show He effects in the implanted layer near the NiAl coating. The procedure involved mounting the TEM disk between two half cylinders of Cu wire with thermal setting epoxy and slicing the composite wire using a slow speed saw equipped with a diamond-impregnated blade to produce 3 mm disks, with the TEM slice supported between the half-cylinders of Cu. Each composite disk was then dimple ground to a central thickness of ~100 μm, and ion milled using a Gatan Precision Ion Polishing System. Ion milling was performed with 5 kV Ar ions to perforation, followed by ion polishing at 2 kV for up to 1800 s to minimize Ar ion damage near the surface. Microstructural examinations were performed on a JEOL 2010F operating at 200 keV in transmission.

Representative regions in the TEM images were selected to determine He bubble number densities and size distributions. Stereo pair images at ~500 nm underfocus were acquired so that the bubbles appeared white with a black outer ring. Foil thickness was measured from stereo pairs using a Hilger–Watts viewer for the center of each region analyzed. A square area centered on the thickness measurement location was analyzed for each specimen. The area analyzed was 0.05304, 0.1380 and 0.003812 μm^2 for specimens R16, R27 and R06, respectively. Grayscale TEM images were converted to black and white images, taking care not to change the shape or size of the bubbles during the conversion. Bubbles appear white against a black background in the converted images. A public domain software package, ImageJ, was used to determine bubble area. Bubble diameters and size distributions were calculated from the area measurements assuming spherical bubbles.

The He concentration was measured in two samples taken from specimen R25. One sample was abrasively polished to remove only the NiAl coating, and the other was abrasively polished to remove

Table 1
Summary of the NiAl coated Eurofer-97 transmission electron microscope discs irradiated in the JP26 experiment

Nominal NiAl thickness, μm	300 °C, 3.9 dpa		400 °C, 3.9 dpa		500 °C, 9 dpa	
	Spec. nos.	[He], appm	Spec. nos.	[He], appm	Spec. nos.	[He], appm
0	R00, R01	0, 0	R10, R11	0, 0	R20, R21	0, 0
1	R02, R03	25, 23	R12, R13	24, 24	R22, R23	98, 98
2	R04, R05	41, 40	R14, R15	40, 40	R24, ***R25***	167, 169
4	***R06***, R07	89, 82	***R16***, R17	82, 81	R26, ***R27***	338, 372

Bold italic specimen numbers denote the samples examined in this study. The He concentrations are expected values based on pre-test calculations.

both the NiAl coating and enough of the Eurofer-97 to leave only the He implanted layer. Prior to analysis, each of these pieces was cut in half, then rinsed in acetone, and air-dried. The mass of each specimen was determined using a calibrated microbalance. Mass uncertainty is estimated to be ±0.001 mg.

The He content of each specimen was determined by isotope-dilution gas mass spectrometry following vaporization in a resistance-heated graphite crucible [6]. The absolute amount of ^{4}He released was measured relative to a known quantity of added ^{3}He 'spike'. The ^{3}He spike was obtained by expanding and partitioning a known quantity of gas through a succession of calibrated volumes [7]. The mass spectrometer was calibrated for mass sensitivity during each series of runs by analyzing known mixtures of ^{3}He and ^{4}He.

3. Results

Fig. 1(a) and (b) gives TEM images showing the microstructure in the He implanted layer for specimen R06. This specimen was irradiated at 300 °C to a dose of 3.9 dpa with a nominal 4 μm layer of NiAl. The expected implanted He concentration for this specimen is ~89 appm. The imaging conditions in Fig. 1(a) were selected to enhance bubble contrast to aid identification and measurement. In Fig. 1(b) dislocation contrast imaging conditions were employed to determine if He bubbles are preferentially associated with dislocations. Detailed bubble size and number density analysis reveals that the mean bubble diameter is ~0.9 nm with a standard deviation (1σ) of 0.2 nm (see Table 2). The measured bubble number density is $\sim 3.6 \times 10^{23}$ m^{-3}. It should be noted the foil thickness measurement for R06 is uncertain. The value reported here is an average of the values for R16 and R27. Due to the very small sizes of the 'black spot' defects produced at 300 °C it was difficult to determine the precise character of these defects. It is presumed they are small dislocation loops. The defect distribution in Fig. 1(b) suggests that loop and/or void formation at 300 °C may have been suppressed by the formation of a high-density of small He bubbles or clusters that served as point defect recombination centers. To explore this possibility the microstructure in the He implanted zone was compared to the microstructure in a He free region of the same specimen, see Fig. 1(c). While the image in Fig. 1(c) was taken at a different magnification there was an indication that loop formation was suppressed in the He implanted zone. This indication needs to be confirmed.

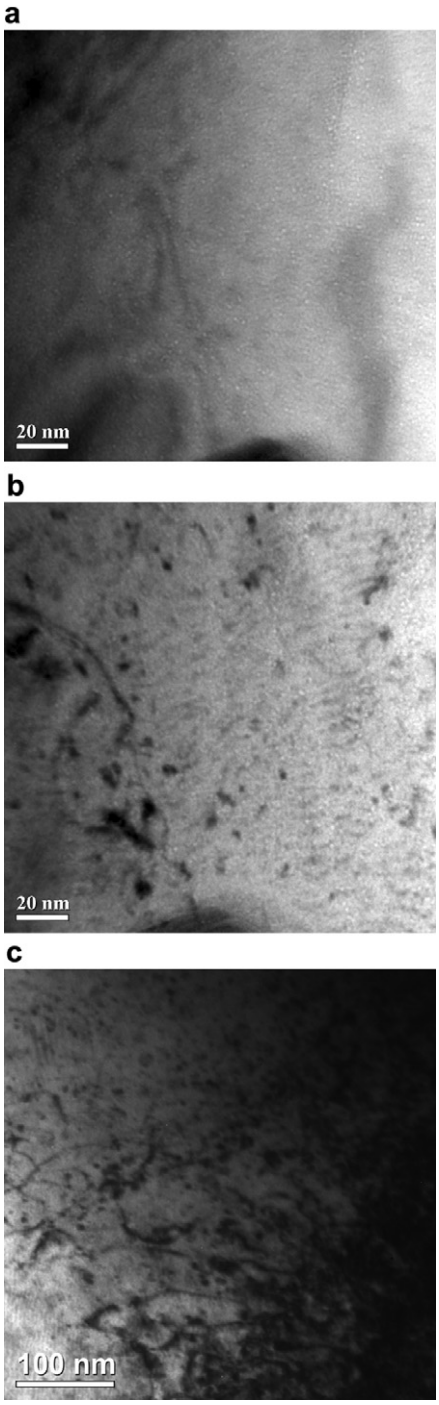

Fig. 1. TEM image showing: (a) the bubble microstructure, (b) the dislocation microstructure and (c) a region with no implanted He far from the ~4 μm NiAl coating for specimen R06 irradiated at 300 °C to a dose of 3.9 dpa. The expected He concentration in (a) and (b) is 89 appm.

Table 2
Measured He bubble sizes and number densities

Specimen no.	Temperature (°C)	Foil thickness (nm)	Mean bubble diameter (nm)	Number density (m^{-3})	No. of helium atoms	He conc. (appm)
R06	300	150[a]	0.9 ± 0.2	3.6×10^{23}	64	270
R16	400	130	3.0 ± 1.4	1.2×10^{22}	909	128
R27	500	170	4.3 ± 1.6	1.5×10^{22}	2186	384
MA957	500	18–131	0.9 ± 0.3	3.0×10^{23}	35	122

Also the calculated He concentration based on the average bubble diameter and number density. Note the MA957 specimen was examined in a companion study and included here for comparison to the Eurofer-97 results [3].
[a] Foil thickness measurement is uncertain. The value reported here is an average of the measurements for R16 and R27.

The bubble and dislocation microstructures for specimen R16 are presented in Fig. 2(a) and (b), respectively. This specimen was irradiated at 400 °C to a dose of 3.9 dpa. The expected concentration of He in the implanted layer was ~82 appm. It is clear that much larger bubbles, at significantly lower density, form at this temperature compared to 300 °C. The mean bubble diameter is 3.0 nm with a standard deviation of 1.4 nm. This is roughly three times larger than at 300 °C with a larger dispersion in bubble sizes. In addition, the bubble number density is 1.2×10^{22} m^{-3} which is about 30 times smaller than at 300 °C. Dislocation loops of both $(a/2)\langle 1\,1\,1\rangle$ and $a\langle 1\,0\,0\rangle$ character were produced at 400 °C. Careful examination of Fig. 2(b) suggests that He bubbles nucleated on pre-existing dislocations.

Fig. 3(a) and (b) illustrates the bubble and dislocation microstructures found in specimen R27 irradiated at 500 °C. This specimen received a dose of 9 dpa, consequently the expected He concentration is 372 appm. The largest He bubbles were observed at this temperature. The mean bubble diameter is 4.3 nm with a standard deviation of 1.6 nm. The mean bubble diameter increased more than 40% relative to R16, but the dispersion of bubble sizes was approximately the same. Bubble number density is slightly larger than for R16 at 1.5×10^{22} m^{-3}. While more than four times as much He was injected into this specimen compared to R06 and R16 the main effect was to increase bubble size rather than increase the number density. It is evident from Fig. 3(a) and (b) that bubbles are associated with dislocations. The 'pearls-on-a-string' bubble arrangements clearly follow pre-existing dislocation patterns.

The results of the He measurements are given in Table 3, and are listed as total atoms of ^{4}He released and as ^{4}He concentrations in atomic parts per million (10^{-6} atom fraction). In Table 3, the samples consisting of only the He implanted layers are identified as R25A, B-thin and samples consisting of the full thickness TEM disc less the NiAl coating are designated as R25C,D-thick. Conversion from total He to He concentration was based on a calculated

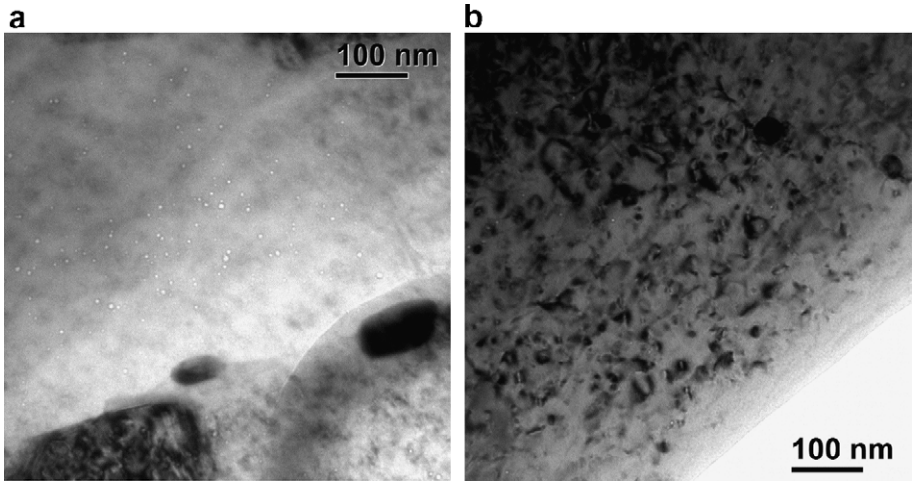

Fig. 2. TEM image showing: (a) the bubble microstructure and (b) the dislocation microstructure for specimen R16 coated with 4 μm of NiAl and irradiated at 400 °C to a dose of 3.9 dpa. The expected He concentration is 82 appm.

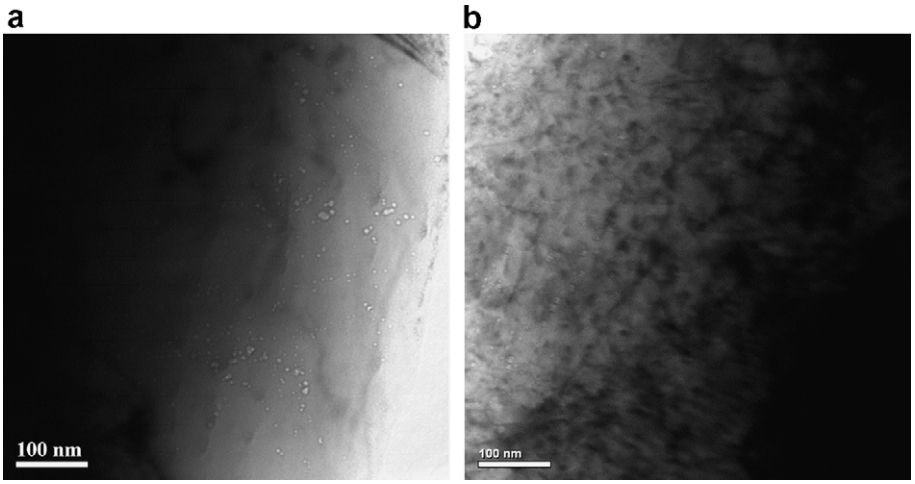

Fig. 3. TEM image showing: (a) the bubble microstructure and (b) the dislocation microstructure for specimen R27 coated with 4 μm of NiAl and irradiated at 500 °C to a dose of 9 dpa. The expected He concentration is 372 appm.

Table 3
The He concentration in R25 measured by a high-sensitivity isotope-dilution magnetic sector mass spectrometer

Specimen ID	Mass[a] (mg)	Measured ^{4}He (10^{14} atoms)	He concentration (appm)[b]	
			Measured	Average[c]
R25A-thin	0.013	0.184	132	132 ± 0.0
R25B-thin	0.022	0.310	132	
R25C-thick	1.138	1.556	12.8	12.2 ± 0.9
R25D-thick	1.127	1.395	11.6	

Specimens denoted as 'thin' were prepared by sanding away the NiAl layer and enough of the Eurofer-97 to leave only the He implanted layer. Specimens denoted as 'thick' were prepared by removing only the NiAl layer leaving both the implanted and unimplanted Eurofer-97.
[a] Mass of specimen for analysis. Mass uncertainty is ±0.001 mg.
[b] Helium concentration in atomic parts per million (10^{-6} atom fraction) with respect to the total number of atoms in the specimen.
[c] Mean and standard deviation (1σ) of duplicate analyses.

value of 1.07×10^{22} atoms/g for Eurofer-97. It should be noted that this value, and the He concentrations obtained using it, are not very sensitive to small changes in material composition.

Mean He contents in the two samples were 132 appm for the thin specimens and 12.2 appm for the thick specimens. The 132 appm value is reasonably close to that calculated for the experiment (see Table 1). The lower He content in the thick samples represents dilution by the much lower He levels in the bulk material away from the implanted layer.

Absolute uncertainty (1σ) in the individual He atom results, determined from the cumulative uncertainties in the isotope ratio measurement, and the spike size, is estimated to be ~1%. For the He concentrations, the sample mass normally contributes negligibly to the final uncertainty. However, for the thin specimens, additional mass uncertainty of ~6% is present due to the very small sample size. The estimated uncertainties are consistent with the variability observed in duplicate analyses.

4. Discussion

As indicated in Table 2 the mean bubble diameter increased systematically with increasing irradiation temperature, and the bubble density at 400 and 500 °C was about 25 times smaller than at 300 °C. Measurements of the He concentration in R25 correlate well with the concentration expected from pretest calculations (132 appm measured versus 169 appm predicted). Measurement of the He concentration in a full-thickness specimen that includes both the He injected zone and the He free region corroborate this result.

We recognize that the minimum bubble sizes observed are near the TEM resolution limit, so the

precise nature of the bubble size distribution is uncertain below that limit. In addition, further work is needed to confirm that specimen preparation procedures, or the presence of surface oxides did not influence our measurements. To provide additional confidence in our results we calculated the He concentration in the injected layer based on the measured average bubble sizes and number densities. We assume that all bubbles were in equilibrium at the irradiation temperature and that the bubble pressure, P, is given by

$$P = \frac{2\gamma}{\langle r \rangle}, \quad (1)$$

where γ is the surface energy, which is taken to be $\sim 2\ \mathrm{J/m^2}$, and $\langle r \rangle$ is the mean bubble radius. A high-pressure equation-of-state [8] was used to determine the mole fraction of He in bubbles at pressure P. We also assume that all of the injected He is contained in the visible bubble population. The estimated He concentrations for R06, R16 and R27 are 270, 128 and 384 appm, respectively (see Table 2). Recall that the expected He levels are 89, 82, and 372 appm. Except for R06 the estimated He concentrations are in fair agreement with expected values. Uncertainty in the foil thickness estimate for R06, coupled with the difficulty of accurately determining the mean bubble size and number density for the very small bubbles in R06 are likely responsible for the difference between the calculated and expected He concentrations.

An objective of our research is to develop and test models of He trapping in ferritic alloys in order to design microstructures with optimal resistance to dimensional instabilities and mechanical property degradation due to He. It is informative to compare the efficiency of He trapping in a nanostructured ferritic alloy such as MA957 with a conventional RAFM alloy such as Eurofer-97. In a companion study [3], NiAl coatings were applied to TEM discs of MA957 and irradiated under the same conditions as R27. The measured bubble sizes and number densities for the MA957 specimen are included in Table 2 for comparison with the present results. While the measured mean bubble size is below the TEM resolution limit, and therefore uncertain, the MA957 results clearly illustrate that a high-density of nano-scale Y–Ti–O particles effectively trapped He and dramatically suppressed bubble growth. Indeed, the measured bubble density is on the same order as the Y–Ti–O particle density. Considering the uncertainty in the bubble size and density measurements for the MA957 specimen, the calculated He concentration is reasonably consistent with the expected value (see Table 2).

5. Conclusions

The He implanter method is an effective experimental approach for producing controlled He-to-dpa ratios in Eurofer-97 under neutron irradiation. Helium bubbles were found in the implanted region with estimated mean diameters of ~0.9, 3.0, and 4.3 nm at 300, 400 and 500 °C, respectively. At 500 °C 10 nm faceted cavities were also observed, which may be voids. Minimum bubble sizes were near the TEM resolution limit for the 300 °C specimen. Loop and void formation at 300 °C may have been suppressed by a high-density of small He bubbles serving as point defect recombination centers. At 400 and 500 °C pre-existing dislocations appear to be preferred He bubble nucleation sites. The addition of a high-density of nano-scale Y–Ti–O particles to a ferritic matrix effectively trapped He atoms and suppressed bubble growth. Additional work is needed to confirm that specimen preparation procedures or surface oxides did not effect results.

Acknowledgements

This research was supported by the US Department of Energy, Office of Fusion Energy Sciences, under contracts DE-AC06-76RLO1830 and DE-FG03-94ER54275, and by the US Department of Energy, Office of Nuclear Energy under contract DE-FC07-051D14663.

References

[1] G.R. Odette, J. Nucl. Mater. 141–143 (1986) 1011.
[2] L.K. Mansur, W.A. Coghlan, in: N.H. Packan, R.E. Stoller, A.S. Kumar (Eds.), Effects of Radiation on Materials: 14th International Symposium, ASTM STP 1046, vol. 1, American Society for Testing and Materials, Philadelphia, 1989, p. 315.
[3] T. Yamamoto, G.R. Odette, P. Miao, D.T. Hoelzer, J. Bentley, N. Hashimoto, H. Tanigawa, R.J. Kurtz, J. Nucl. Mater., in press, doi:10.1016/j.jnucmat.2007.03.047.
[4] R.E. Stoller, H. Tanigawa, Fusion Materials Semiannual Progress Report for Period Ending June 30, 2003, DOE/ER-0313/34 (2003) 142.
[5] K.R. Thoms, D.W. Heatherly, S.H. Kim, R.G. Sitterson, R.E. Stoller, Fusion Materials Semiannual Progress Report for Period Ending December 31, 2003 DOE/ER-0313/35, 2004, p. 250.
[6] H. Farrar, B.M. Oliver, J. Vac. Sci. Technol. A 4 (1986) 1740.
[7] B.M. Oliver, J.G. Bradley, H. Farrar, Geochim. Cosmochim. Acta 48 (1984) 1759.
[8] R.E. Stoller, G.R. Odette, J. Nucl. Mater. 131 (1985) 118.